Solar Energy Materials & Solar Cells 254 (2023) 112281

Contents lists available at ScienceDirect

Solar Energy Materials and Solar Cells

journal homepage: www.elsevier.com/locate/solmat

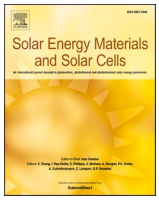

Viability of intermediate band solar cells based on InAs/GaAs submonolayer quantum dots and the role of surface reconstruction

T. Borrely [a,*], A. Alzeidan [a], M.D. de Lima [a], G.M. Jacobsen [b], T.-Y. Huang [c], Y.-C. Yang [c], T.F. Cantalice [a], R.S. Goldman [c], M.D. Teodoro [b], A.A. Quivy [a]

[a] Institute of Physics, University of São Paulo, Rua do Matão 1371, 05508-090, São Paulo, SP, Brazil
[b] Department of Physics, Federal University of São Carlos, 13565-905, São Carlos, SP, Brazil
[c] Department of Materials Science & Engineering, University of Michigan, Ann Arbor, MI, USA

ARTICLE INFO

Keywords:
Submonolayer quantum dot
Intermediate band solar cell
InAs
GaAs
Molecular beam epitaxy

ABSTRACT

The effects of growth conditions on InAs/GaAs submonolayer-quantum-dot solar cells are still a little explored topic, and the literature shows contradictory results regarding the efficiency of these devices. Through electrical and optical characterizations (photoluminescence, current-voltage curves, and external quantum efficiency) and self-consistent Schrödinger–Poisson simulations in the effective-mass approximation, we investigate how the reconstruction of the GaAs(001) surface prior to the deposition of InAs/GaAs submonolayer quantum dots influences the properties of these nanostructures and the performance of solar cells. Current-voltage characteristics and external quantum efficiency curves show that the use of the (2 × 4) surface reconstruction—instead of the commonly used c(4 × 4) surface reconstruction—leads to higher short-circuit current density and improved performance at room temperature. The (2 × 4) surface reconstruction also leads to enhanced photoluminescence intensity at low temperatures compared to the c(4 × 4) surface reconstruction. The simulations—which are based on previous cross-sectional scanning tunneling microscopy data of InAs/GaAs submonolayer quantum dots—indicate that neither type of submonolayer quantum dot can confine electrons, as they are too small and their In content is too low. However, the electron ground state is closer to being confined in the SMLQDs grown with the (2 × 4) surface reconstruction, as such nanostructures are surrounded by a thick InGaAs layer having a lower In content than for the other surface reconstruction. The discussion presented herein elucidates a contradiction between different reports found in the literature regarding the conversion efficiency of InAs/GaAs submonolayer-quantum-dot solar cells and indicates possible ways forward for achieving 3D electron confinement in these devices.

1. Introduction

It has been over 25 years since Luque and Martí introduced the concept of intermediate-band solar cell (IBSC) [1]. In short, the IBSC model adds three premises [2] to those adopted by Shockley and Queisser in their efficiency-limit study [3]: (A) An energy band is present in the bandgap of the solar-cell (SC) host material. Thus, three transitions are allowed for electrons to absorb photons: from the valence band (VB) to the intermediate band (IB), from the IB to the conduction band (CB), and the usual one, from the VB to the CB. Consequently, the short-circuit current density (J_{sc}) is expected to increase relative to a SC without an intermediate band. (B) The density of states between the VB and the IB as well as the one between the IB and the CB are null, therefore a quasi Fermi level can be ascribed to each of the three bands. (C) The IB does not reach the contacts of the device, i.e., holes and electrons can only be collected after they are excited to the VB and the CB, respectively. If assumptions (B) and (C) are met, the IBSC is expected to preserve its open-circuit voltage (V_{oc}), i.e., V_{oc} will not be limited by the energy difference between the valence-band edge and the intermediate band [2]. This does not imply, however, that the IBSC will not have some V_{oc} degradation relative to its conventional counterpart, as the introduction of an intermediate band unescapably increases recombination in the device, even if only radiative. Hence, at low sunlight concentrations, some V_{oc} degradation is expected in the IBSC, and a beyond-Shockley-Queisser efficiency is predicted only whenever the expected J_{sc} gain substantially outweighs the V_{oc} loss [4–6].

* Corresponding author.
E-mail address: thales.santos@usp.br (T. Borrely).

https://doi.org/10.1016/j.solmat.2023.112281
Received 2 December 2022; Received in revised form 25 February 2023; Accepted 3 March 2023
Available online 13 March 2023

For the last two decades, numerous attempts to produce an IBSC with higher conversion efficiency (η) than conventional SCs have been made [6–19], most of them involving InAs Stranski-Krastanov quantum dots (SKQDs) to create an intermediate band in III-V SCs [7–14]. We will henceforth refer to this kind of device as SKQD IBSC. Despite efforts, the introduction of such nanostructures consistently resulted in substantial V_{oc} degradation and, consequently, in efficiency loss, even though there were reports of modest improvements in Jsc [7,10]. Several causes for this poor performance have been proposed [6]: (1) tunneling between the IB and the CB as a consequence of the intense electric field in the p-n junction [14]; (2) a high capture rate of electrons from the CB by the QDs [20]; (3) a thermal energy connection between the IB and the CB due to the energy levels of the QDs being too shallow [21]; (4) Shockley-Read-Hall (SRH) recombination due to the defects caused by strain in the surroundings of the SKQDs [22].

Problems (1) and (2) can be solved with simple structure-design adjustments [6]. Inserting the QDs into the intrinsic layer of a p-i-n junction—instead of using a p-n junction—weakens the built-in electric field and hampers electrons from tunneling out of the QDs. Doping the QDs increases their occupancy factor and decreases their electron capture rate. Problems (3) and (4) are harder to circumvent, as they are more closely related to the self-assembly process of SKQDs over which the device designer has limited control. There are reports of attempts to deal with (3) by using $Al_xGa_{1-x}As$ barriers and GaAs [13] or InGaP [12] matrixes to make the differences between the energy bands approach theoretically optimized values. As to (4), partial V_{oc} recovery and/or enhanced photoluminescence have been achieved through rapid thermal annealing [21,23,24], strain-balance layers [7], In-flush [11], and capping procedures [11,23–25]. The use of GaP strain-balance layers was the most successful of these, as it led to a V_{oc} loss of only 47 mV (4.5%) relative to a reference device [7]. Although all these attempts found at least some degree of success in improving the quality of SKQDs and SKQD IBSCs, none of them resulted in a device with a higher conversion efficiency than its conventional counterpart, which motivates the research of other techniques to grow epitaxial quantum dots.

The submonolayer deposition is an alternative to the SK growth technique. InAs/GaAs submonolayer quantum dots (SMLQDs) are produced by repeating a two-step cycle [26,27]: first, a fraction of a monolayer (ML) of InAs material is deposited on a GaAs surface; second, a few monolayers of GaAs are grown on top. Ideally, the first step results in the nucleation of small 1-ML-high InAs islands all over the surface, and the second step covers these islands and provides a new GaAs surface for the next period. As the cycle is repeated, the subsequent set of two-dimensional (2D) InAs islands tends to nucleate vertically aligned to the previous one due to the strain field originating from the lattice mismatch between both materials. Thus, in an ideal scenario, a SMLQD is a columnar structure containing *N* 2D InAs islands separated by a few monolayers of GaAs, where *N* is the number of cycle repetitions (Fig. 1). For simplification, we will adopt the notation *N* × [Material A(thickness of A in MLs)/Material B(thickness of B in MLs)] to refer to specific SMLQDs—e.g., SMLQDs deposited by repeating four times a two-step cycle of 0.5 ML of InAs followed by 1.5 MLs of GaAs will be referred to as 4 × [InAs(0.5)/GaAs(1.5)]. A priori, SMLQDs have several advantages that suggest they might be suitable substitutes for SKQDs in IBSCs, to form what we will henceforth refer to as SMLQD IBSCs. SMLQDs consist of stacks of small 2D InAs islands whose areal density can reach the 10^{12} cm^{-2} range [28]. This is almost two orders of magnitude higher relative to SKQDs [29]. Therefore, they could lead to a substantial increase in J_{sc} and quantum efficiency in the GaAs sub-bandgap range. Additionally, a lower concentration of crystalline defects is expected in SMLQDs due to their peculiar planar growth. More precisely, in the SML technique, In deposition stops before the formation of a wetting layer—an unavoidable feature of SKQDs [30] that increases the elastic energy stored in the system and contributes to inhibiting the quasi-Fermi level splitting in IBSCs—thus lowering the strain surrounding the SMLQDs when compared to SKQDs. Finally, in contrast with SKQDs, the height and composition of SMLQDs can be tuned by changing the number of cycles, thickness, and composition of layers, allowing more control over the intermediate-band energy, which could contribute to the splitting of the IB and CB quasi-Fermi levels.

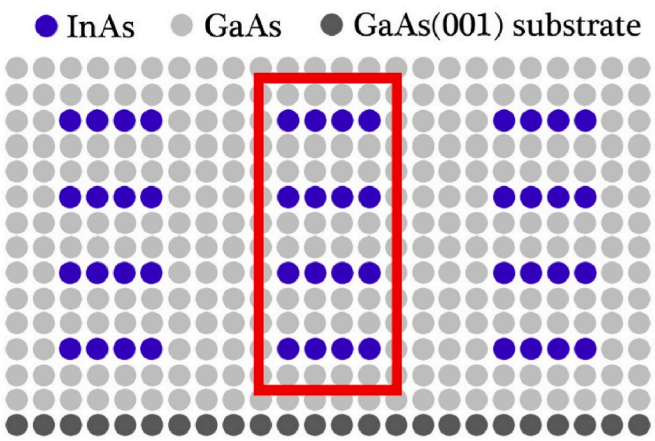

Fig. 1. Schematic of InAs/GaAs submonolayer quantum dots formed by four repetitions of a two-step cycle consisting of 0.5 ML of InAs followed by 2.5 MLs of GaAs, i.e., 4 × [InAs(0.5)/GaAs(2.5)]. The red box identifies a single ideal SMLQD.

In practice, however, growing SMLQDs is not as simple as it might look at first glance. Characterizations of InAs/GaAs SMLQDs showed no clear evidence of vertical alignment of 2D InAs islands [31–33]. Furthermore, a strong segregation effect causes In atoms to spread in the thin GaAs spacer layers [31–33]. Consequently, the submonolayer technique results in a dot-in-well structure, i.e., $In_xGa_{1-x}As$ clusters (SMLQDs) embedded in an $In_yGa_{1-y}As$ quantum well (QW), with $x > y$ [31–33]. In addition, the areal density of SMLQDs tends to be lower than the areal density of the first 2D InAs islands formed in the first step of the growth cycle [32,33], and an increase in the cycle repetition number does not necessarily lead to a proportional increase in cluster height [31,32]. Photoluminescence and magneto photoluminescence characterizations in combination with Schrödinger–Poisson simulations in the effective-mass approximation and eight-band $k \bullet p$ calculations indicated that this dot-in-a-well structure tends to cause a heterodimensional carrier confinement—i.e, electrons are confined in the QW or across multiple SMLQDs, whereas holes are confined in a single SMLQD [31]. Cross-sectional scanning tunneling microscopy (XSTM) characterizations demonstrated that the surface reconstruction (SR) of GaAs immediately prior to the deposition of 6 × [InAs(0.5)/GaAs(2.5)] SMLQDs strongly influences the cluster and QW atomic arrangements. More precisely, they demonstrated that the (2 × 4) SR leads to lower SMLQD areal density, lower total In concentration, and lower In concentration in the QW [32,33]. Since the present work uses these same types of InAs/GaAs SMLQDs, we can thus take full advantage of these XSTM results.

A few studies [15–18] on InAs/GaAs-SMLQD IBSCs and ternary variations of these compound semiconductors can be found in the literature. In all of them, GaAs-based p-i-n structures containing SMLQDs in the middle of the intrinsic layer were grown by molecular beam epitaxy. It was reported that a small amount of Sb ($x = 0.05$) in 6 × [InAs(0.5)/$GaAs_{1-x}Sb_x$(2.5)] SMLQDs caused a small V_{oc} loss but also an enhancement in J_{sc} and η in comparison to a device with no Sb [16], which the authors attributed to an improvement in the crystal quality at the heterointerfaces caused by the Sb surfactant effect. Different works showed that InAs/GaAs-SMLQD IBSCs outperformed InAs-SKQD IBSCs [17,18]—mainly due to the former presenting higher V_{oc}—and $In_{0.16}Ga_{0.84}As$-quantum-well (QW) IBSCs [15,18] in all figures of merit. A study reported that 12 × [InAs(0.25)/GaAs(1.25)] SMLQDs and 6 × [InAs(0.5)/GaAs(2.5)] SMLQDs led IBSCs to be more efficient than a

quantum-dot-free control device, as an increase in J_{sc} caused by the nanostructures was not accompanied by a proportional V_{oc} loss [18]. Contrastingly, however, a different report showed that 6 × [InAs (0.5)/GaAs(2.5)] SMLQDs caused a minor J_{sc} loss and a substantial V_{oc} degradation relative to a reference solar cell [15].

This literature on InAs/GaAs-SMLQD IBSCs is still sparse and, thus, has several gaps that need to be filled. For example, there is a lack of discussions on the InAs/GaAs-SMLQD growth conditions (temperature, fluxes, and surface reconstruction) and their effects. We believe, however, that such discussions are of great importance given that there is clear evidence of the influence of the growth conditions on the properties of InAs/GaAs SMLQDs [32,33]. Bearing this in mind, our objective here is to compare different SMLQD IBSCs containing InAs/GaAs SMLQDs with the same nominal structure but grown under different conditions. More precisely, we will assess the effects of SR on InAs/GaAs-SMLQD IBSCs through optical and electrical characterizations, and self-consistent Schrödinger–Poisson simulations in the effective-mass approximation.

2. Materials and methods

Four devices were grown by molecular beam epitaxy on semi-insulating GaAs(001) substrates (Fig. 2). All of them were p-i-n junctions with highly-doped n-type back-surface-field layers, back contact layers, and front contact/surface-field layers. Si and C were used for n and p doping, respectively. All layers were made of GaAs grown at 570 °C. The only differences between devices were the presence/absence of InAs/GaAs QDs in the middle of the intrinsic layer and their growth parameters. The first device, used as a reference, had no QDs; the second one, named *SK SC*, had InAs SKQDs; the other two had 6 × [InAs(0.5)/GaAs(2.5)] SMLQDs grown on a (2 × 4) or a c(4 × 4) GaAs(001) surface, and they were respectively named *(2×4) SC* and *c(4×4) SC*. All QD devices had 10 layers of QDs separated by 40 nm of GaAs. The SKQDs were obtained by depositing 2.2 MLs of InAs:Si at 515 °C and immediately covered with 10 nm of GaAs at the same temperature to avoid In evaporation. These nanostructures were doped with four Si atoms per QD in order to fill the defect states around the dots and to fill half of the QDs ground state. The SKQD areal density was previously established by atomic force microscopy to be 4×10^{10} cm^{-2}. The last 30 nm of the GaAs spacer were grown at 570 °C. The InAs and GaAs growth rates were respectively 0.096 ML/s and 0.98 ML/s; the As flux was equivalent to 1.8 ML/s. The SMLQDs were grown at 490 °C and immediately capped with 3 nm of GaAs also grown at 490 °C followed by 37 nm of GaAs at 570 °C. Due to their planar growth, SMLQDs are expected to produce fewer defects than SKQDs. Thus, the thin GaAs spacer was Si doped with only two Si atoms per QD, assuming an areal density of 4.5×10^{11} cm^{-2} [32]. One should be aware that the real density of defects and areal density of QDs are unknown, thus these doping concentrations are based on estimates. Dedicated studies are required for achieving a true half-filled intermediate band. The c(4 × 4) SMLQDs were grown under the same conditions as the SKQDs, whereas the (2 × 4) SR required a much lower As flux (equivalent to ≈ 0.15 ML/s) and, consequently, a lower deposition rate of InAs (≈0.015 ML/s) and GaAs (≈0.1 ML/s) to maintain an As-rich surface during growth.

It is important to mention here that, although the literature on InAs/GaAs-SMLQD IBSCs does not usually mention detailed growth conditions, the (2 × 4) SR requires fluxes that are drastically lower from the ones commonly used for standard SKQDs. Therefore, it is reasonable to assume that all previous reports on InAs/GaAs-SMLQD IBSCs have used the c(4 × 4) SR, and that this is the first study applying 6 × [InAs(0.5)/GaAs(2.5)] SMLQDs grown on a (2 × 4) GaAs(001) surface to solar cells.

Optical lithography and wet etching were used to define 4.83 mm^2 mesas. Ni/Ge/Au and Pt/Ti/Au thin films were evaporated by e-beam to produce n- and p-type metal contacts, respectively, that became Ohmic after rapid thermal annealing at 520 °C for 30 s. The contact area accounted for 11% of the front surface. Illuminated and dark I–V characteristics were obtained with a Sun 3000 Class AAA solar simulator at 298 K. Illuminated I–V curves were measured under AM1.5G spectrum. External-quantum-efficiency (EQE) spectra were obtained with a Si photodetector and a globar as radiation source to improve the signal-to-noise ratio in the near-infrared range. The PL measurements were performed from 10 K to 240 K with a 19.2 μW solid-state laser emitting at 730 nm on GaAs samples containing quantum dots grown under the same conditions used for our quantum dot solar cells. The optical signal was detected with a Si CCD and an InGaAs diode-array detector for SMLQDs and SKQDs, respectively.

3. Experimental results

The best illuminated I–V characteristics of each device type are presented in Fig. 3 and summarized in Table 1 (row "best device"). They show that the reference SC has the best performance, whereas the SK SC has the worst one. The poor performance of the SK SC is mostly due to substantial V_{oc} and FF degradations. In agreement with other works [17,

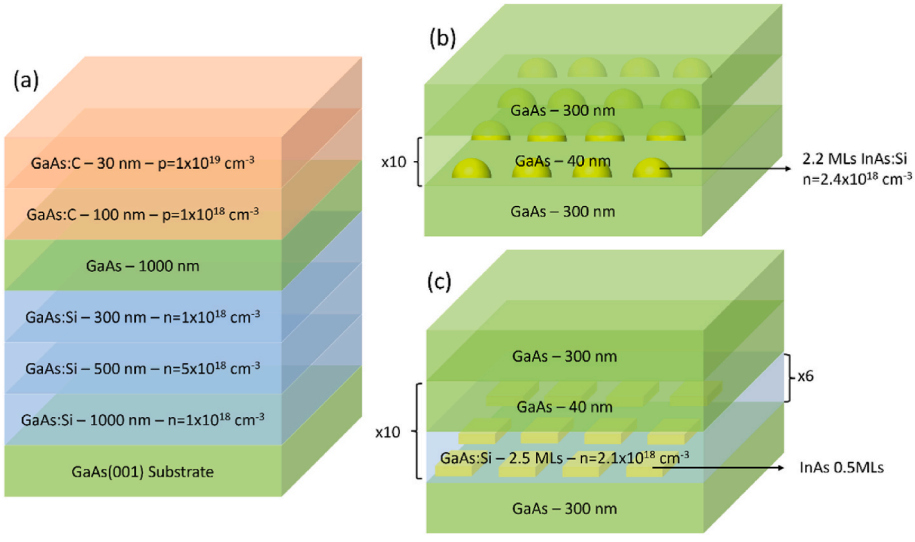

Fig. 2. Schematic of the four solar cells that only differ by their intrinsic region. (a) Full layer structure of the reference sample; (b) intrinsic region of the SK SC; (c) intrinsic region of both SMLQD SCs. The difference between them is the reconstruction of the GaAs(001) surface prior to deposition of the SMLQDs ((2 × 4) or c(4 × 4)).

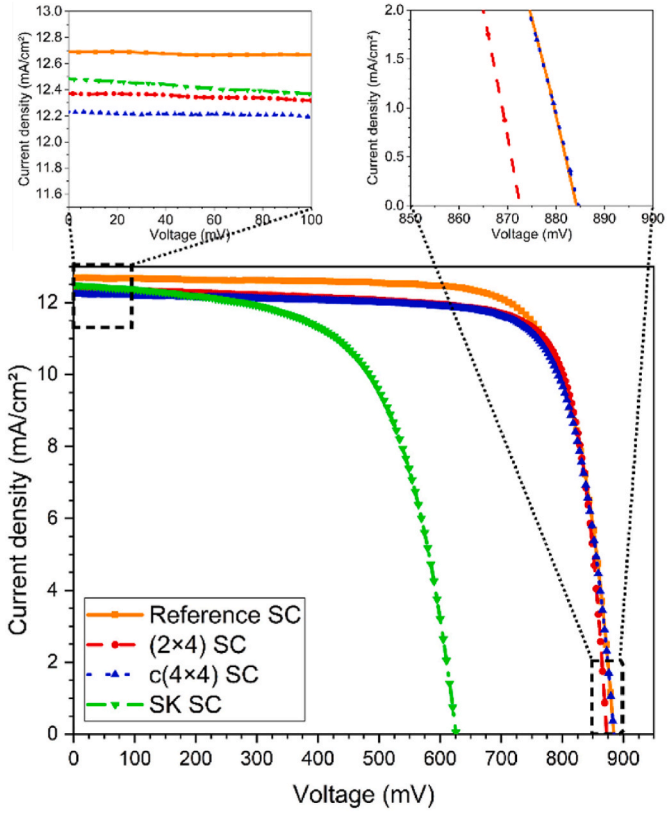

Fig. 3. Illuminated I–V curves of the best device of each type obtained under AM1.5G illumination and 298K.

Table 1
Mean and uncertainty of the figures of merit of all solar cells and figures of merit of the best of each device type. *N* is the number of analyzed devices.

Analysis type	Parameter	ReferenceSC	(2 × 4) SC	c(4 × 4) SC	SK SC
Best device	J_{sc} (mA/cm²)	12.7	12.4	12.2	12.5
	V_{oc} (mV)	887	872	884	627
	FF (%)	78.1	78.8	77.5	59.9
	η (%)	8.8	8.5	8.4	4.7
	J_0 (mA/cm²)	2.1×10^{-11}	1.1×10^{-10}	7.0×10^{-11}	3.5×10^{-6}
	N	1.8	1.9	1.8	2.9
Statistical	J_{sc} (mA/cm²)	12.67(3)	12.44(5)	11.98(5)	12.64 (6)
	V_{oc} (mV)	882.53(93)	864.9 (20)	863.3 (66)	598.8 (62)
	FF (%)	76.51(34)	74.60 (73)	74.2(12)	60.16 (36)
	η (%)	8.55(3)	8.03(8)	7.68(16)	4.55(6)
	N	28	17	16	16

18], the (2 × 4) SC and the c(4 × 4) SC present only minor V_{oc} degradations and, consequently, considerably outperform the SK SC.

In Fig. 4, the dark I–V characteristics of the same devices from Fig. 3 were fitted in the high-voltage range using the single-diode model:

$$J = J_0\left(e^{\frac{qV}{nkT}} - 1\right) \quad (1)$$

where J is the dark current density, q is the elementary charge, k is the Boltzmann constant, T is the absolute temperature, J_0 is the dark saturation current density, and n is the ideality factor. The dark I–V results are also summarized in Table 1 (row "best device"). The SK SC has the highest J_0 by far (3.5×10^{-6} mA/cm²), a few orders of magnitude higher

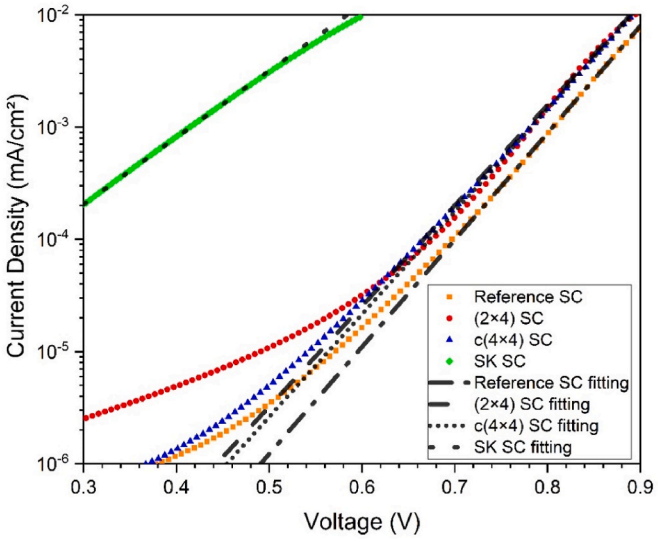

Fig. 4. Dark I–V curves of the best device of each type at 298 K.

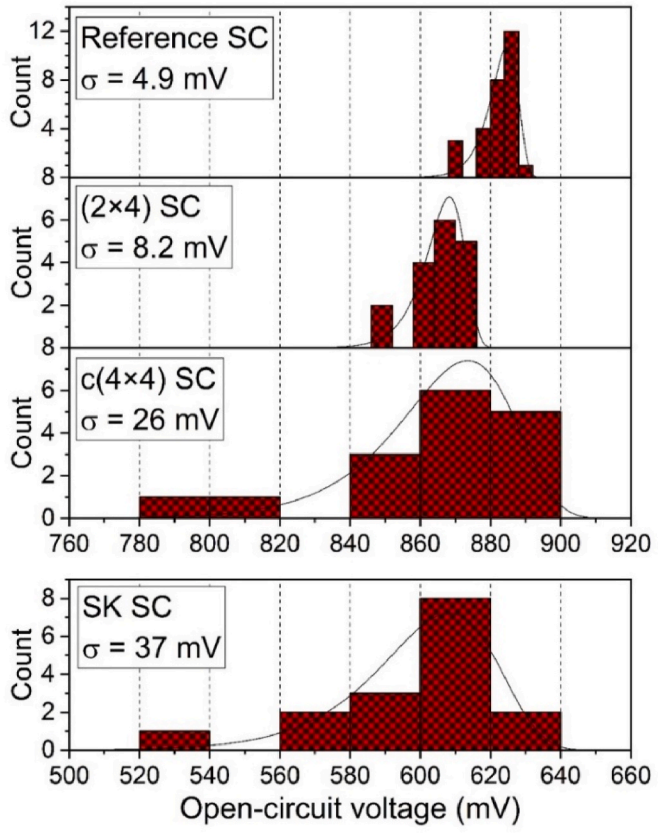

Fig. 5. V_{oc} histograms of all solar cells separated by device type.

than the other devices. The (2 × 4) SC and the c(4 × 4) SC have similar J_0 values (1.1×10^{-10} mA/cm² and 7.0×10^{-11} mA/cm², respectively), which are slightly higher relative to the reference SC (2.1×10^{-11} mA/cm²). Regarding the ideality factor, the SK SC is the only one that has $n > 2$, and all the other devices present similar n values within the typical 1–2 range (Table 1). Considering that J_0 and n are, respectively, quantitative and qualitative indicators of recombination and that $n > 2$ can be a sign of multiple-defect recombination being a dominant mechanism [34], these results are in full agreement with the V_{oc} values found in Fig. 3 and with the expected high and low levels of non-radiative

recombination in SKQDs and SMLQDs, respectively.

An important feature seen in Fig. 3 is how small the differences between some figures of merit of the different solar cells are. Indeed, the literature on SMLQD IBSCs indicates that the differences between performances of conventional SCs and SMLQD IBSCs under standard conditions tend to be small, especially the V_{oc} difference, that is typically in the range of tens of millivolts but might be even smaller [15–18]. Table 1 (row "statistical") shows the means and uncertainties of all figures of merit calculated from several devices of each type. By comparing the best-device analysis to the statistical one, it is clear that some of the features of Fig. 3 are not representative of the data set and could lead to misleading conclusions if analyzed alone. Thus, a statistical comparison between device types—instead of a direct comparison between the best device of each type—is best suited here to identify and understand the influence of growth methods and conditions on performance.

Even when considering statistical fluctuations, the most efficient device still is the reference SC followed by the (2 × 4) SC, c(4 × 4) SC, and SK SC, respectively. However, the poor performance of the SK SC is now exclusively due to a V_{oc} loss, as its J_{sc} is compatible with that of the reference SC. The open-circuit voltages of the (2 × 4) SC and the c(4 × 4) SC are not significantly different from each other but are higher relative to the SK SC and slightly lower (difference smaller than 20 mV) in comparison to the reference SC. The V_{oc} degradation of these SMLQD devices is smaller than those found SKQD IBSCs [7–14]. Again, this agrees with the expected low density of defects in the SMLQD SCs. Regarding J_{sc}, the SMLQD devices perform worse than the other ones, and the (2 × 4) SC performs better than the c(4 × 4) SC.

Although over a dozen solar cells of each type were analyzed, the V_{oc} uncertainty of the QD devices is still in the order of mV, a substantial value compared to the small performance differences between conventional and SMLQD devices reported in the literature [15–18]. V_{oc} histograms for each solar cell type are presented in Fig. 5. All distributions are negatively skewed with standard deviation (σ) ranging from a few mV to tens of mV. The samples with higher In concentration also have a higher standard deviation, thus there seems to be a positive correlation between σ and In concentration. Although the mean V_{oc} of the reference SCs is visibly the highest among all device types, due to its high standard deviation, the right-side tail of the c(4 × 4) distribution is even further right relative to the reference-SC distribution. Therefore, a best-device comparison is expected to increase the chances of concluding that the c(4 × 4) SC is as good as, or even better than, the reference SC, despite the mean of the former being lower. This could explain why conflicting reports are indicating SMLQD IBSCs with 6 × [InAs(0.5)/GaAs(2.5)] SMLQDs performing worse [15] and better [18] than their conventional counterparts.

Although all three QD devices have wider EQE ranges than the reference SC (Fig. 6), the latter has the highest EQE above the bandgap. This is consistent with the reference having the highest J_{sc}. The sub-bandgap EQEs of the QD SCs are typical of the VB-IB absorption in InAs/GaAs quantum-dot solar cells [5]. The SK SC has the widest EQE range (~1100 nm), which contributes to its J_{sc} being higher in comparison to the SMLQD devices. The EQE range of the c(4 × 4) SC (975 nm) is approximately 28 nm wider than that of the (2 × 4) SC (947 nm).

Photoluminescence results (Fig. 7) show that the optical emission related to the ground states of the SKQDs, c(4 × 4) SMLQDs, and (2 × 4) SMLQDs is maximum at 1.145 eV, 1.380 eV, and 1.387 eV, respectively. The SKQDs also present an excited state at 1.209 eV. For a solar cell, a lower ground state energy means a smaller energy difference between IB and VB. Thus, QDs with lower emission energies are expected to lead to higher EQE ranges. This is exactly what we see comparing Figs. 6 and 7. The redshift of the c(4 × 4) sample relative to the (2 × 4) sample, although minor (only 7 meV), is consistent with the former SR leading to a higher total In concentration [32]. The SKQDs emission is redshifted approximately 240 meV relative to the SMLQDs, an expected result given that the nominal In concentration of InAs SKQDs is higher and their size is much larger in comparison to InAs/GaAs SMLQDs [35]. It is worth noting that the PL intensity of the (2 × 4) SC is substantially higher compared to the c(4 × 4) SC. This difference, however, quickly fades away as the temperature increases (Fig. 8).

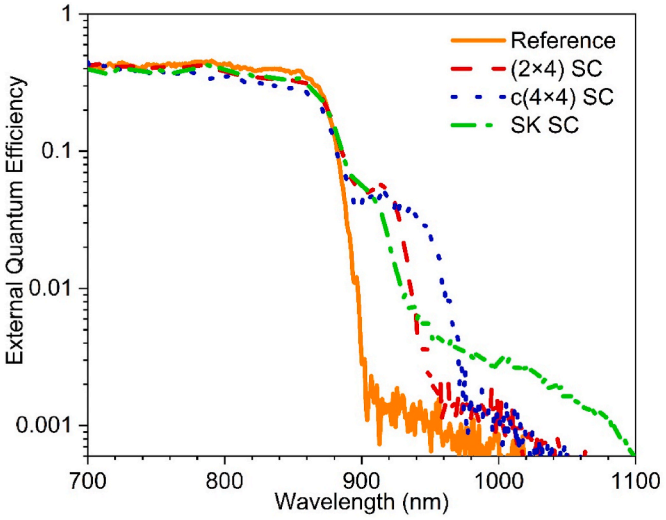

Fig. 6. External quantum efficiency of the best device of each type.

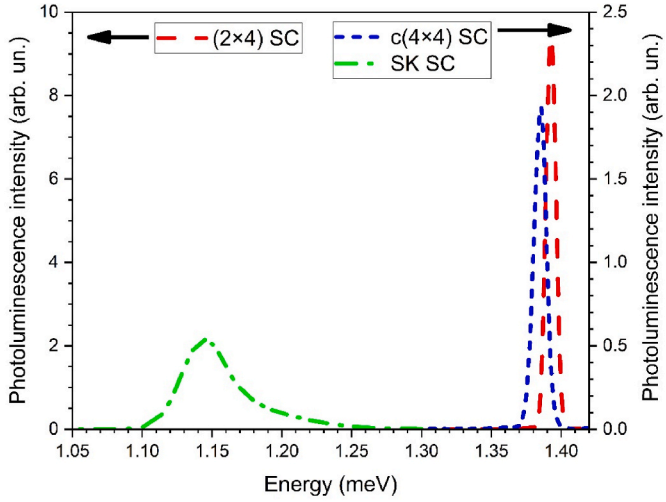

Fig. 7. Photoluminescence spectra at 10K of samples containing QDs grown in the same conditions as those present in the active region of the three QD SCs.

4. Numerical results and discussion

In a nutshell, our results show that, independently of the GaAs SR prior to the SMLQD deposition, 6 × [InAs(0.5)/GaAs(2.5)] SMLQDs lead, with statistical significance, to devices with extended absorption, small J_{sc} loss, small V_{oc} degradation, and a slight increase of carrier recombination with respect to a conventional SC. In comparison to SKQDs, again independently of the SR, 6 × [InAs(0.5)/GaAs(2.5)] SMLQDs resulted in shorter absorption range, small J_{sc} loss, substantial V_{oc} recovery, and much lower carrier recombination. Let us now turn our attention to the main point of contention in this work, i.e., how SR affects QDs and device properties and what can be learned from these effects.

Comparing the (2 × 4) SC to the c(4 × 4) SC, we see that the former is more efficient than the latter exclusively due to a non-negligible J_{sc} gain, as their V_{oc} are not significantly different. In quantum-dot-based IBSCs, higher quantum-dot areal density is a possible cause for J_{sc} improvement, as it increases the number of channels for sub-bandgap photon

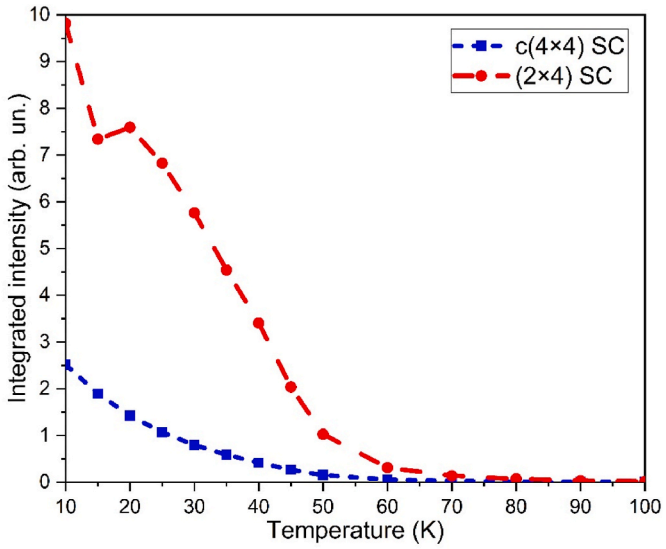

Fig. 8. PL intensity of the two types of InAs/GaAs SMLQD as a function of temperature.

absorption. However, it has been demonstrated that there is roughly a tenfold decrease in the areal density of 6 × [InAs(0.5)/GaAs(2.5)] SMLQDs with the (2 × 4) SR compared with that of the c(4 × 4) SR [32,33], thus ruling out this possibility. A more consistent explanation is the higher (lower) ground-state energy resulting from the lower (higher) In concentration caused by the (2 × 4) SR (c(4 × 4) SR), as a shallower (deeper) ground state is expected to facilitate (hamper) both thermal and photon-assisted electron escape from IB to CB.

Naturally, one might question why the higher areal density of SMLQDs in the c(4 × 4) SC does not result in higher J_{sc}, sub-bandgap EQE, and PL intensity. In Fig. 7, one can see that SMLQDs have a single electronic bound state, which, due to their small size and low In concentration, is very close to the top of the potential barrier, causing the wave function of confined electrons to be only weakly localized [31,33]. Given that the first nearest neighbor distance between SMLQDs is in the order of a few nm for both SRs [32,33], in the best-case scenario, there will be an overlap of the electronic ground-state wave function of the closest SMLQDs. Then, by the Pauli exclusion principle, once an electron occupies a SMLQD, the probability of neighbor SMLQDs also being occupied should drastically decrease. In the worst-case scenario, the ground-state energy is so shallow that electrons are not at all confined in the SMLQDs, but only in the surrounding QW—at 298 K, the temperature at which the I–V characteristics and EQE were measured, this is the most likely possibility [31]. In either case, the higher number of SMLQDs in the c(4 × 4) SC will not manifest in any benefit to device performance.

Notwithstanding that these considerations about electron confinement explain why one should not expect the c(4 × 4) SC to have an enhanced PL, they do not account for the higher PL intensity of the (2 × 4) SC at low temperatures. PL intensity is essentially determined by the probability of carriers recombining radiatively. Therefore, in principle,

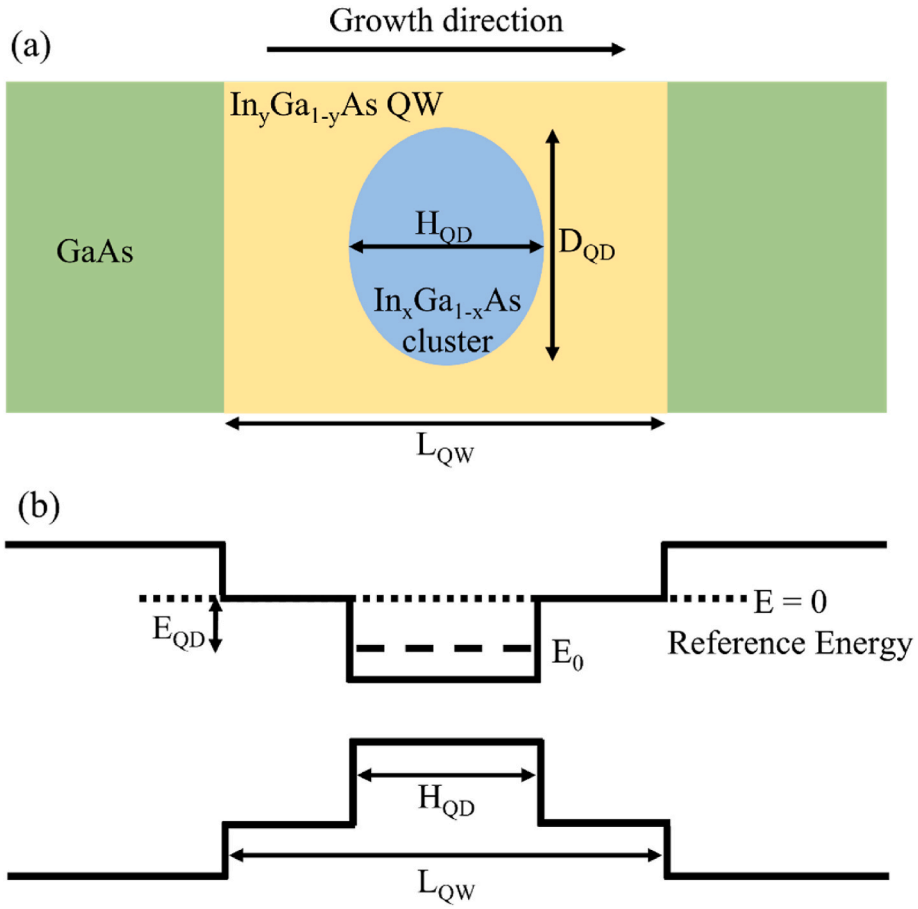

Fig. 9. (a) Model of a SMLQD for self-consistent Schrödinger–Poisson simulations in the effective-mass approximation consisting of an $In_xGa_{1-x}As$ cluster in an $In_yGa_{1-y}As$ quantum well, both in a GaAs matrix. (b) Band diagram of the SMLQD model. The in-dot electron confinement energy, E_{QD}, is the difference between the electron ground-state energy, E_0, and the reference energy, i.e., the conduction-band edge of the quantum well. Therefore, if the electron is confined in the QD, $E_{QD} \leq 0$ meV.

the presence of more non-radiative recombination centers in the c(4 × 4) SC could be responsible for its lower PL intensity. However, this is an unlikely possibility, as defects also lead to V_{oc} degradation and higher J_0, none of which are true as reported in Table 1.

To investigate this matter, we computed the electronic states of a simple model with a single quantum dot in a quantum well (Fig. 9) using self-consistent Schrödinger–Poisson simulations in the effective-mass approximation. Based on XSTM images [32,33], the dot was assumed to be elliptical with a xy-plane diameter (D_{QD}) of 6 nm and a height (H_{QD}) of 5 nm. The nominal thickness of the SMLQD region in our samples is approximately 5 nm (18 MLs), but In segregation makes the real thickness larger; thus, we adopted 6 nm for the well thickness (L_{QW}). The nominal In composition in our $In_xGa_{1-x}As$ SMLQDs is $x = 0.33$, and the nominal In composition of the surrounding $In_yGa_{1-y}As$ QW is $y = 0.00$. Although XSTM characterizations cannot provide precise compositional information, they have unambiguously proven that the (2 × 4) SR leads to a decrease in y relative to the c(4 × 4) SR [32,33]. How the SR affects x, however, is not as clear, as the QD signal overlaps the QW signal in cross-sectional images. On the one hand, given that the XSTM results show that part of the InAs material from the 2D InAs islands is scattered in the QW around the SMLQDs ($y > 0$), due to mass conservation, we should then expect the In content in the SMLQDs to be substantially lower than its nominal value. On the other hand, the XSTM images also show that the thin GaAs layers separating vertically the 2D InAs islands inside each SMLQD were replaced by InGaAs material as well. Therefore, we cannot rule out the possibility that SMLQDs might have an In content close to the nominal value, and we will adopt $x \leq 0.33$ in our simulation.

In Fig. 10, we plot the difference between the electronic ground-state energy and quantum-well conduction-band-edge energy (we call it in-dot electron confinement energy, E_{QD}) as a function of x and y. Initially, for the sake of simplicity and comparison with the literature, strain was not considered. Due to their larger mass, holes are more easily confined than electrons [31]—if the conditions allow electrons confinement, holes will certainly be confined as well—and therefore are not a point of concern in our calculations. The ranges of interest ($0.29 < x < 0.33$ and $0.04 < y < 0.10$) were determined by identifying the region around $E_{QD}(x, y) = 0$ meV—i.e., the region in which the electronic wave function of the ground state changes from in-dot confined ($E_{QD} < 0$ meV, blue-green color) to in-well confined ($E_{QD} > 0$ meV, red-black color)—that meets the upper limit restriction of x.

The results show that electronic in-dot confinement is only possible if $y \lesssim 0.08$. The x range is small, meaning that the $In_xGa_{1-x}As$ clusters cannot lose much In relative to their nominal x value if one wishes to obtain electronic in-dot confinement. Furthermore, the plane equation

$$E_{QD} = -414x + 663y + 84 \quad (2)$$

is a good approximation of E_{QD} in the analyzed range ($R^2 = 0.999$). The negative x and positive y coefficients imply that confinement is favored by an increase of In concentration in the QD and a decrease of In concentration in the QW. In terms of absolute values, the y coefficient (663 meV) is 60% higher than the x coefficient (414 meV), suggesting that confinement is more affected by composition changes in the QW than in the QD. Given that XSTM images indicate that the (2 × 4) SR leads to a clear reduction in y in comparison to the c(4 × 4) SR, the E_{QD} of the (2 × 4) SC is most likely lower than the E_{QD} of the c(4 × 4) SC even if the decrease in y is accompanied by a similar decrease in x.

Confinement and localization in nanostructures are closely related to PL intensity, as the probability of carrier recombination depends on the overlap between hole and electron wavefunctions [35–37]. In InAs/-GaAs SMLQDs, the higher the difference between x and y—or, equivalently, the closer the electron ground state is to confinement—the more localized the electron ground state wave function is [31]. In other words, the electron ground state wavefunction spreads across a smaller number of SMLQDs if the difference between x and y increases. Therefore, electrons in the (2 × 4) SC are expected to be more localized compared to the c(4 × 4) SC, leading to the higher PL intensity seen in Fig. 7 and 8.

Harrison et al. arrived, qualitatively, at the same results in Fig. 10 with a model similar to the one in Fig. 9 [31]. They assumed perfectly spherical SMLQDs (diameter = 5 nm), a thicker QW (well thickness = 13 nm), and concluded that in-dot electron confinement was only possible for $x \gtrsim 0.32$ if $y = 0$—in other words, 6 × [InAs(0.5)/GaAs(2.5)] SMLQDs are capable of confining electrons only if their x and y real values are close to the nominal values. However, neither their calculations nor Fig. 10 take strain into account. In the InAs/GaAs system, strain reduces the conduction band offset between InAs and GaAs [38], making electron confinement even more difficult to achieve. Therefore, it should not be neglected in our analysis. In Fig. 11, we repeated the calculations presented in Fig. 10 but, this time, taking strain into account. In this case, in-dot electron confinement cannot be achieved (E_{QD} is always larger than zero) in 6 × [InAs(0.5)/GaAs(2.5)] SMLQDs with

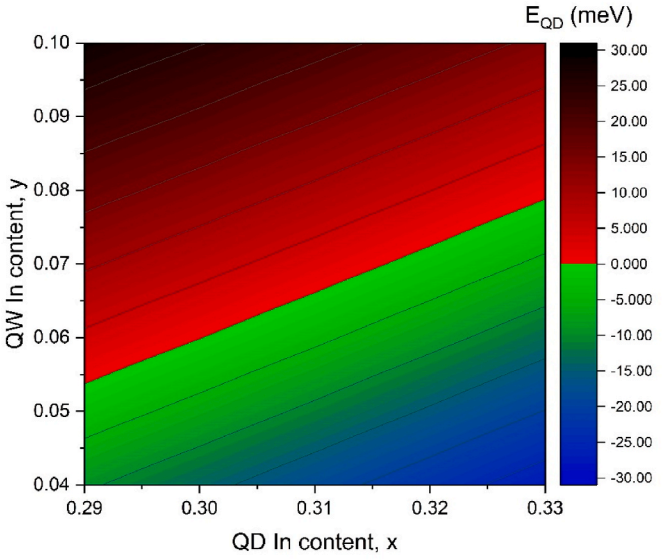

Fig. 10. Simulated in-dot electron confinement energy (E_{QD}) as a function of quantum-well and quantum-dot In content without considering strain. Blue-green colors represent in-dot confinement ($E_{QD} \leq 0$), while red-black colors represent in-well confinement ($E_{QD} > 0$).

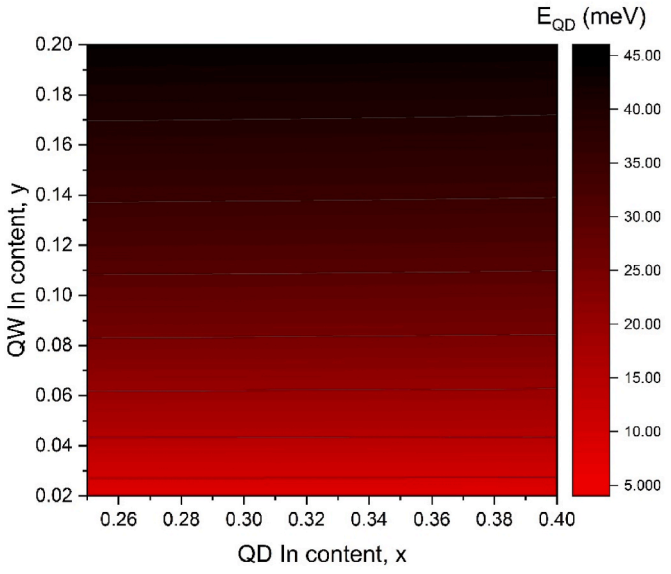

Fig. 11. Simulated in-dot electron confinement energy (E_{QD}) as a function of quantum-well and quantum-dot In content considering strain. In-dot confinement ($E_{QD} \leq 0$) is not viable in the analyzed range.

the dimensions reported in the XSTM studies [32,33]. A decrease in y still contributes to in-dot electron confinement—the analysis regarding electron localization and PL intensity should hold—but the contour lines in Fig. 11 are practically horizontal, i.e., E_{QD} is barely affected by changes in x in the range of interest, as the QDs are too small to confine electrons.

To further investigate the possibility of in-dot electron confinement, we ran self-consistent Schrödinger–Poisson simulations in the effective-mass approximation to calculate E_{QD} as a function of the SMLQD dimensions (xy-plane diameter and height) while considering strain. Our goal is to assess whether electron confinement is possible in the best-case scenario for InAs/GaAs SMLQDs, as Fig. 10 and 11 suggest that SMLQDs must be larger and have a higher In content for $E_{QD} < 0$ to be achieved. In terms of growth process, a higher nominal x value can be obtained, for instance, by reducing the thin GaAs interlayer from 2.5 MLs to 1.5 MLs, in which case x goes from 0.33 to 0.50. Thus, in Fig. 12 we take $x = 0.50$. We assume a good vertical alignment of the InAs islands by taking the well thickness to be the same as the QD height and $y = 0.05$. We should mention that segregation is expected to make the QW width a few nanometers larger than the QD height. Consequently, when we assume $L_{QW} = H_{QD}$, we are neglecting the influence of segregation. Our decision is not based on the assumption that segregation can be fully inhibited, but on the fact that the size of the QW surrounding the QD has little impact on the electron confinement in the QD, i.e., the influence of L_{QW} on E_{QD} is negligible. The results show that, even with such a high In content, for symmetrical nanostructures (i.e., height = width), the QDs must be approximately 9 nm wide. For $H_{QD} = 5$ nm, $E_{QD} < 0$ meV only if $D_{QD} \gtrsim 13$ nm. For $D_{QD} = 5$ nm, $E_{QD} > 0$ meV even for $H_{QD} = 20$ nm. Furthermore, the first partial derivative of E_{QD} with respect to D_{QD} is higher compared to the first partial derivative with respect to H_{QD}, meaning that E_{QD} is more affected by changes in D_{QD} than in H_{QD}.

For high-efficiency IBSCs, despite resulting in enhanced radiative recombination in the QDs, in-dot electron confinement at room temperature is necessary because the absence of phonon-bottleneck effect in quantum wells allows a connection between the electrons in the conduction band and those in the intermediate band, hampering the quasi-Fermi-level splitting [39]. In summary, Fig. 11 and 12 show that 6 × [InAs(0.5)/GaAs(2.5)] SMLQDs cannot confine electrons, and for in-dot electron confinement to become a possibility: (I) InAs/GaAs SMLQDs require a higher In content; (II) InAs/GaAs SMLQDs must be larger; (III) Improving the vertical alignment of the In(Ga)As islands is not enough, it is also necessary to find ways of nucleating In(Ga)As islands that have a larger lateral size.

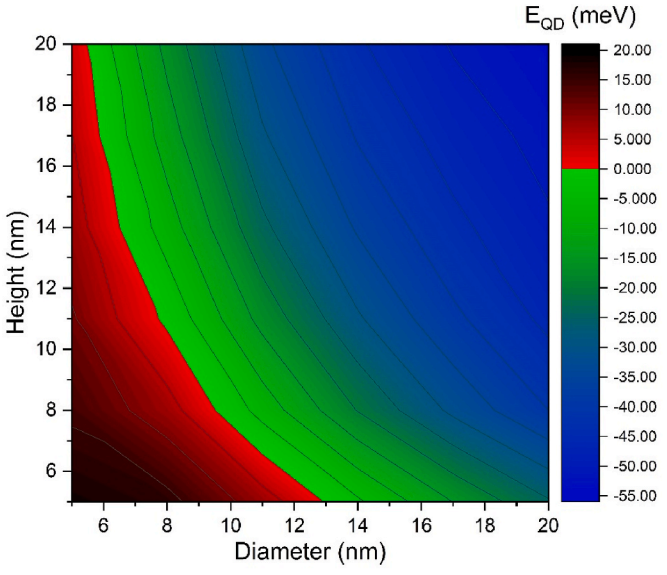

Fig. 12. Simulated in-dot electron confinement energy as a function of diameter (xy-plane size) and height (z-direction size) of $In_xGa_{1-x}As$ clusters in an $In_yGa_{1-y}As$ quantum well, with $x = 0.50$, $y = 0.05$, and well thickness = cluster height. Blue-green colors represent in-dot confinement ($E_{QD} \leq 0$), while red-black colors represent in-well confinement ($E_{QD} > 0$).

One can think of a few ways of exploring new growth conditions and parameters to address these issues. Reducing the submonolayer-cycle thickness to 2 monolayers instead of 3 should increase the In content (issue I)—i.e., one could grow N × [InAs(A)/GaAs(2-A)] SMLQDs instead of N × [InAs(A)/GaAs(3-A)] SMLQDs. Consequently, it could improve the vertical alignment (the higher the In content, the stronger the strain field [40]) and the height of SMLQDs (issue II). Lower growth temperatures could reduce In segregation, which is a thermally activated process, leading to higher In content (issue I) and improved vertical alignment as well (issue II) [40]. Increasing the InAs coverage—i.e., using a deposition scheme like N × [InAs(A)/GaAs(2-A)] with A > 0.5 ML—could cause the In(Ga)As islands to coalesce, therefore increasing D_{QD} (issue III). Such exploration, however, will require characterization techniques capable of providing compositional information at the nanoscale [41–43].

5. Conclusion

In conclusion, we investigated GaAs-based solar cells containing InAs SKQDs and 6 × [InAs(0.5)/GaAs(2.5)] SMLQDs. Our findings corroborate the literature on SMLQDs that shows that devices based on this type of nanostructure outperform SKQD-based devices due to the latter presenting a higher loss by non-radiative recombination that leads to substantial V_{oc} degradation. In the course of this analysis, we realized, through the use of simple statistical tools, that contradictions between different reports in the literature on the performance of IBSCs containing 6 × [InAs(0.5)/GaAs(2.5)] SMLQDs—grown with the c(4 × 4) SR—are most likely a consequence of statistical fluctuations. Our results indicate that the use of the (2 × 4) SR instead of the c(4 × 4) SR improves quantum efficiency, short-circuit current, and conversion efficiency, but neither SR leads to enhanced efficiency at 298 K and AM1.5G conditions relative to a control device. The (2 × 4) SR, however, resulted in enhanced PL at low temperature (T < 70 K) compared to the c(4 × 4) SR. Through numerical calculations, we demonstrated that this is possibly caused by an improved electron localization in SMLQDs grown with the (2 × 4) SR, as this SR leads to a lower In concentration in the QW surrounding the In-rich $In_xGa_{1-x}As$ clusters, causing the electron ground-state energy to be closer to the QW conduction-band edge. Lastly, we showed that, for 3D electron confinement to be possible, InAs/GaAs SMLQDs need to be a few nanometers larger and have a higher In content relative to the 6 × [InAs(0.5)/GaAs(2.5)] SMLQDs analyzed here. The growth conditions of InAs/GaAs SMLQDs are still a little explored topic, and our results point some ways forward for further investigations of this matter.

CRediT authorship contribution statement

T. Borrely: Writing – original draft, Visualization, Validation, Software, Methodology, Investigation, Formal analysis, Data curation, Conceptualization. **A. Alzeidan:** Investigation. **M.D. de Lima:** Investigation. **G.M. Jacobsen:** Investigation, Formal analysis, Data curation. **T.-Y. Huang:** Validation, Software. **Y.-C. Yang:** Visualization, Software. **T.F. Cantalice:** Investigation. **R.S. Goldman:** Writing – review & editing, Supervision, Resources, Funding acquisition. **M.D. Teodoro:** Supervision, Resources, Funding acquisition. **A.A. Quivy:** Writing – review & editing, Supervision, Resources, Project administration, Funding acquisition.

Declaration of competing interest

The authors declare that they have no known competing financial

interests or personal relationships that could have appeared to influence the work reported in this paper.

Data availability

Data will be made available on request.

Acknowledgments

This study was financed in part by the Coordenação de Aperfeiçoamento de Pessoal de Nível Superior – Brasil (CAPES) – Finance Code 001, and by CNPq (grants 309837/2021-9 and 157446/2017-4). The authors also acknowledge the financial support of the Fundação de Amparo à Pesquisa do Estado de São Paulo (FAPESP) – grants 2018/06328-1, 2014/19142-2, and 2015/19210-0. TYH, YCY, and RSG gratefully acknowledge support from the U.S. National Science Foundation (Grant No. DMR 1810280).

References

[1] A. Luque, A. Martí, Increasing the efficiency of ideal solar cells by photon induced transitions at intermediate levels, Phys. Rev. Lett. 78 (1997) 5014, https://doi.org/10.1103/PhysRevLett.78.5014.
[2] Í. Ramiro, A. Martí, Intermediate band solar cells: present and future, Prog. Photovoltaics Res. Appl. 29 (2020) 705–713, https://doi.org/10.1002/pip.3351.
[3] W. Shockley, H.J. Queisser, Detailed balance limit of efficiency of p-n Junction solar cells, Appl. Phys. 32 (1961) 510, https://doi.org/10.1063/1.1736034.
[4] Í. Ramiro, A. Martí, E. Antolín, A. Luque, Review of experimental results related to the operation of intermediate band solar cells, IEEE J. Photovoltaics 4 (2014) 736–748, https://doi.org/10.1109/JPHOTOV.2014.2299402.
[5] E. López, et al., Demonstration of the operation principles of intermediate band solar cells at room temperature, Sol. Energ. Mat. Sol. C. 149 (2016) 15–18, https://doi.org/10.1016/j.solmat.2015.12.031.
[6] Í. Ramiro, et al., Analysis of the intermediate-band absorption properties of type-II GaSb/GaAs quantum-dot photovoltaics, Phys. Rev. B 96 (2017), 125422, https://doi.org/10.1103/PhysRevB.96.125422.
[7] C.G. Bailey, D.V. Forbes, R.P. Raffaelle, S.M. Hubbard, Near 1 V open circuit voltage InAs/GaAs quantum dot solar cells, Appl. Phys. Lett. 98 (2011), 163105, https://doi.org/10.1063/1.3580765.
[8] N.S. Beattie, et al., Quantum engineering of InAs/GaAs quantum dot based intermediate band solar cells, ACS Photonics 4 (2017) 2745–2750, https://doi.org/10.1021/acsphotonics.7b00673.
[9] F.K. Tutu, et al., Improved performance of multilayer InAs/GaAs quantum-dot solar cells using a high-growth-temperature GaAs spacer layer, J. Appl. Phys. 111 (2012), 046101, https://doi.org/10.1063/1.3686184.
[10] S.A. Blokhin, et al., AlGaAs/GaAs photovoltaic cells with an array of InGaAs QDs, Semiconductors 43 (2009) 514–518, https://doi.org/10.1134/S1063782609040204.
[11] E. Weiner, et al., Effect of capping procedure on quantum dot morphology: implications on optical properties and efficiency of InAs/GaAs quantum dot solar cells, Sol. Energ. Mat. Sol. C. 178 (2018) 240–248, https://doi.org/10.1016/j.solmat.2018.01.028.
[12] Í. Ramiro, et al., Wide-bandgap InAs/InGaP quantum-dot intermediate band solar cells, IEEE J. Photovoltaics 5 (2015) 840, https://doi.org/10.1109/JPHOTOV.2015.2402439.
[13] R. Jakomin, et al., InAs quantum dot growth on $Al_xGa_{1-x}As$ by metalorganic vapor phase epitaxy for intermediate band solar cells, J. Appl. Phys. 116 (2014), 093511, https://doi.org/10.1063/1.4894295.
[14] E. Antolín, et al., Reducing carrier escape in the InAs/GaAs quantum dot intermediate band solar cell, J. Appl. Phys. 108 (2010), 064513, https://doi.org/10.1063/1.3468520.
[15] P. Lam, et al., Submonolayer InGaAs/GaAs quantum dot solar cells, Sol. Energ. Mat. Sol. C. 126 (2014) 83–87, https://doi.org/10.1016/j.solmat.2014.03.046.
[16] Y. Kim, K.-Y. Ban, C. Zhang, C.B. Honsberg, Material and device characteristics of InAs/GaAsSb sub-monolayer quantum dot solar cells, Appl. Phys. Lett. 107 (2015), 153103, https://doi.org/10.1063/1.4933272.
[17] I.S. Han, J.S. Kim, J.O. Kim, S.K. Noh, S.J. Lee, Fabrication and characterization of InAs/InGaAs sub-monolayer quantum dot solar cell with dot-in-a-well structure, Curr. Appl. Phys. 16 (2016) 587–592, https://doi.org/10.1016/j.cap.2016.02.009.
[18] N. Alnami, et al., InAs nanostructures for solar cell: improved efficiency by submonolayer quantum dot, Sol. Energ. Mat. Sol. C. 224 (2021), 111026, https://doi.org/10.1016/j.solmat.2021.111026.
[19] S. Huang, A.V. Semichaevsky, L. Webster, H.T. Johnson, R.S. Goldman, Influence of wetting layers and quantum dot size distribution on intermediate band formation in InAs/GaAs superlattices, J. Appl. Phys. 110 (2011), 073105, https://doi.org/10.1063/1.3631785.
[20] K. Sablon, et al., Effective harvesting, detection, and conversion of IR radiation due to quantum dots with built-in charge, Nanoscale Res. Lett. 6 (2011) 584, https://doi.org/10.1186/1556-276X-6-584.
[21] P. Lam, et al., InAs/InGaP quantum dot solar cells with an AlGaAs interlayer, Sol. Energ. Mat. Sol. C. 144 (2016) 96–101, https://doi.org/10.1016/j.solmat.2015.08.031.
[22] A. Martí, et al., Emitter degradation in quantum dot intermediate band solar cells, Appl. Phys. Lett. 90 (2007), 233510, https://doi.org/10.1063/1.2747195.
[23] J. Saha, et al., Higher performance optoelectronic devices with $In_{0.21}Al_{0.21}Ga_{0.58}As/In_{0.15}Ga_{0.85}As$ capping of III-V quantum dots, J. Lumin. 210 (2019) 75–82, https://doi.org/10.1016/j.jlumin.2019.02.022.
[24] T.V. Torchynska, R.C. Tamayo, G. Polupan, G.I.J.G. Moreno, A.E. Echavarria, Annealing impact on emission of InAs quantum dots in $GaAs/Al_{0.30}Ga_{0.70}As$ structures with different capping layers, J. Electron. Mater. 50 (2021) 4633–4641, https://doi.org/10.1007/s11664-021-09007-2.
[25] D. González, et al., Evaluation of different capping strategies in the InAs/GaAs QD system: composition, size and QD density features, Appl. Surf. Sci. 537 (2021), 148062, https://doi.org/10.1016/j.apsusc.2020.148062.
[26] I.L. Krestnikov, N.N. Ledentsov, A. Hoffmann, D. Bimberg, Arrays of two-dimensional islands formed by submonolayer insertions: growth, properties, devices, Phys. Stat. Sol. (A) 183 (2001) 207–233, https://doi.org/10.1002/1521-396X, 200102)183:2<207::AID-PSSA207>3.0.CO;2-2.
[27] A. Alzeidan, M.S. Claro, A.A. Quivy, High-detectivity infrared photodetector based on InAs submonolayer quantum dots grown on GaAs(001) with a 2 × 4 surface reconstruction, J. Appl. Phys. 126 (2019), 224506, https://doi.org/10.1063/1.5125238.
[28] A. Lenz, et al., Atomic structure and optical properties of InAs submonolayer depositions in GaAs, J. Vac. Sci. Technol. B 29 (2011), 04D104, https://doi.org/10.1116/1.3602470.
[29] A. Schwan, et al., Dispersion of electron g-factor with optical transition energy in (In,Ga)As/GaAs self-assembled quantum dots, Appl. Phys. Lett. 98 (2011), 233102, https://doi.org/10.1063/1.3588413.
[30] I.R. Pagnossin, E.C.F. da Silva, A.A. Quivy, The quantum mobility of a two-dimensional electron gas in selectively doped GaAs/InGaAs quantum wells with embedded quantum dots, J. Appl. Phys. 97 (2005), 113709, https://doi.org/10.1063/1.1925329.
[31] S. Harrison, et al., Heterodimensional charge-carrier confinement in stacked submonolayer InAs in GaAs, Phys. Rev. B 93 (2016), 085302, https://doi.org/10.1103/PhysRevB.93.085302.
[32] R.S.R. Gajjela, et al., Cross-sectional scanning tunneling microscopy of InAs/GaAs (001) submonolayer quantum dots, Phys. Rev. Materials 4 (2020), 114601, https://doi.org/10.1103/PhysRevMaterials.4.114601.
[33] A. Alzeidan, et al., Effect of as flux on InAs submonolayer quantum dot formation for infrared photodetectors, Sens. Actuators, A A. 334 (2022), 113357, https://doi.org/10.1016/j.sna.2021.113357.
[34] O. Breitenstein, et al., Interpretation of the Commonly Observed I-V Characteristics of C-SI Cells Having Ideality Factor Larger than Two, IEEE 4th World Conference on Photovoltaic Energy Conference, 2006, pp. 879–884, https://doi.org/10.1109/WCPEC.2006.279597.
[35] C.A. Duarte, et al., Influence of the temperature on the carrier capture into self-assembled InAs/GaAs quantum dots, J. Appl. Phys. 93 (2003) 6279, https://doi.org/10.1063/1.1568538.
[36] A.M. Ceschin, et al., Photoluminescence and photoreflectance studies on δ-Doped $In_{0.15}Ga_{0.85}As$/GaAs quantum wells, Supelattices and Microstructures 15 (1994) 333–337, https://doi.org/10.1006/spmi.1994.1065.
[37] A. Tabata, et al., Investigation of the photoluminescence linewidth broadening in symmetric and asymmetric InGaAs/GaAs n-type δ-doped quantum wells, Mater. Sci. Eng. B 35 (1995) 401–405, https://doi.org/10.1016/0921-5107(95)01329-6.
[38] R.Y. Tanaka, N.M. Abe, E.C.F. da Silva, A.A. Quivy, A. Passaro, Modeling the 3D in profile of $In_xGa_{1-x}As$/GaAs quantum dots, J. Phys. Appl. Phys. 49 (2016), 215101, https://doi.org/10.1088/0022-3727/49/21/215101.
[39] A. Martí, et al., Novel semiconductor solar cell structures: the quantum dot intermediate band solar cell, Thin Solid Films 511 (2006) 638–644, https://doi.org/10.1016/j.tsf.2005.12.122.
[40] T.F. Cantalice, et al., Evidence of weak strain field in InAs/GaAs submonolayer quantum dots, Micro and Nanostructures 172 (2022), 207449, https://doi.org/10.1016/j.micrna.2022.207449, 2022.
[41] B. Gault, et al., Atom probe tomography, Nature Reviews Methods Primers 1 (2021) 51, https://doi.org/10.1038/s43586-021-00047-w.
[42] T. Borrely, T.-Y. Huang, Y.-C. Yang, R.S. Goldman, A.A. Quivy, On the Importance of Atom Probe Tomography for the Development of New Nanoscale Devices, *2022 36th Symposium On Microelectronics Technology And Devices (SBMicro)*, 2022, pp. 1–4, https://doi.org/10.1109/SBMICRO55822.2022.9881039.
[43] C. Greenhill, et al., Influence of quantum dot morphology on the optical properties of GaSb/GaAs multilayers, Appl. Phys. Lett. 116 (2020), 252107, https://doi.org/10.1063/5.0011094.